AI-Driven Signal Processing for SF6 Circuit Breaker Performance Optimization

Philippe A. V. D. Liz [1,*,†,‡], Giovani B. Vitor [1,*,‡], Ricardo T. Lima [2,‡] and Aurélio L. M. Coelho [1,‡] and Eben P. Silveira [1,‡]

1 Laboratory of Robotics, Intelligent and Complex Systems—ROBSIC, Itabira 35903-087, MG, Brazil; aurelio.coelho@unifei.edu.br (A.L.M.C.); eben@unifei.edu.br (E.P.S.)

2 Centrais Elétricas Brasileiras S/A—ELETROBRÁS, Rio de Janeiro 20091-005, RJ, Brazil; tozzi@eletrobras.com

* Correspondence: varme.dias@gmail.com (P.A.V.D.L.); giovanibernardes@unifei.edu.br (G.B.V.)

† Current address: Institute of Technological Sciences, ICT, Federal University of Itajubá, UNIFEI, Itabira Campus, Itabira 35903-087, MG, Brazil.

‡ These authors contributed equally to this work.

Abstract: This work presents an approach based on signal processing and artificial intelligence (AI) to identify the pre-insertion resistor (PIR) and main contact instants during the operation of high-voltage SF6 circuit breakers to help improve the settings of controlled switching and attenuate transients. For this, the current and voltage signals of a real Brazilian substation are used as AI inputs, considering the noise and interferences common in this type of environment. Thus, the proposed modeling considers the signal preprocessing steps for feature extraction, the generation of the dataset for model training, the use of different machine learning techniques to automatically find the desired points, and, finally, the identification of the best moments for controlled switching of the circuit breakers. As a result, the models evaluated obtained good performance in the identification of operation points above 93%, considering precision and accuracy. In addition, valuable statistical notes related to the controlled switching condition are obtained from the circuit breakers evaluated in this research.

Keywords: high-voltage circuit breakers; artificial intelligence; substation capacitor bank; controlled switching

1. Introduction

High-voltage circuit breakers are critical equipment in a substation (SE), as they are responsible for performing operations to connect and disconnect loads or to isolate the system when faults occur. Failures in this asset can result in serious security and financial losses for sector agents. For this reason, monitoring the main parameters of the circuit breaker becomes essential to anticipate failures and estimate the useful life of the equipment, resulting in economic, operational, and strategic gains [1–3].

During the switching, the circuit breaker is subject to the highest levels of transients depending on the type of load connected to it [4–6].

In circuit breaker operations, particularly those involving capacitor banks [7,8], the synchronization of switching is crucial to minimize transients and protect equipment. During the closing operation, two distinct events occur in sequence: pre-insertion contact and main contact. The pre-insertion contact refers to the moment when the circuit breaker first connects a resistor or another element to limit inrush currents and transients before full conduction [9]. The main contact follows, representing the final closure of the circuit

to enable uninterrupted current flow through the circuit breaker. Identifying these points accurately is essential for ensuring proper operation and minimizing harmful transient effects [10].

Among the problems related to circuit breakers that operate with capacitor banks, one of the main issues is related to controlled switching closing operations, which can generate high levels of inrush current transients associated with high frequencies. These transients cause damage to the circuit breaker itself, the capacitor bank, adjacent equipment, and even remote equipment, leading to premature wear of assets, directly impacting maintenance management and, in the worst case, causing asset unavailability and financial losses [11].

The process of identifying this synchronization is carried out by finding the pre-insertion and main contact points in the current signal, as explored in [10]. This task becomes complex when considering a real system operating in the substation, which is subject to various interferences and noise, such as high transients generated, as well as disturbances caused by the back-to-back effect of operations in the capacitor bank.

Some works published in the last few years explored techniques to improve the synchronization of the switching controller of high-voltage circuit breakers. Motivated by failures in autotransformers between 2005 and 2006 at a real substation, Luz et al. [11] discuss the adjustment of synchronizers in the closing operation of capacitor banks to reduce the current and voltage transients that occurred during the closing of the capacitor bank circuit breakers. Manual transient measurements were taken at the autotransformer terminals, and adjustments were made to the synchronizers to regulate the closing of the circuit breakers to reduce transient currents. Finally, a significant decrease in maximum currents and voltage variations was observed, resulting in less wear on the auxiliary components of the circuit breakers, which increases the reliability and longevity of transformers and capacitor banks.

With the same objective of synchronizing the closing mechanism to reduce transients, Goldsworthy et al. [12] developed a system that determines the insertion points based on the voltage waveform and aligns the closing with the contact operating time at the voltage zero. Unlike other works, it does not use the pre-insertion resistor and implements point-on-wave control to determine timing and synchronization. The work is validated through field experiments, comparing switching data before and after the implementation of control.

Sun et al. [13] investigate controlled switching synchronization using real-time simulations, adjusting and analyzing in detail the impact of different parameters, such as resistor size, insertion angle, and contact operating time. By monitoring the voltage drop between contacts and the sudden increase in current, they can identify the exact moment when the closing occurs, using the dielectric decay rate of the contacts as a reference. They conclude that adjusting the insertion angle and pre-insertion time is essential for effectively mitigating switching transients. However, all operations are performed through simulations that do not consider noise and interferences that occur in a real system.

Liu et al. [14] develop a drive motor and a controller to ensure precision in closing contacts at the zero voltage point. The latter is implemented using a new control approach called FPD (function-switching pseudo-differential), which dynamically adjusts control parameters according to the phase of the circuit breaker contact movement, reducing calculation complexity and improving system response. The insertion point is identified by monitoring the motor rotation and contact movement. This new approach is compared with conventional strategies and demonstrates higher precision and stability in contact closing, with closing errors within ±0.5 ms.

A proposal for calculating the opening and closing times of the main contacts of circuit breakers is presented in [15] through the analysis of voltage and current oscillography

synchronized with the equipment's trip command. Both the Fourier transform and the Wavelet transform were used as analysis techniques. A prototype was installed in a 440 kV substation to monitor the quantities. It should be noted that no intelligent techniques were used to detect possible anomalies in the circuit breaker operation, such as those based on artificial intelligence.

Several intelligent methods have been used to predict and diagnose circuit breaker failures. Some of these works are based on artificial intelligence (AI) and machine learning (ML) techniques. References [16,17] use techniques based on artificial neural networks (ANNs) and support vector machines (SVMs) to evaluate characteristics of the displacement curve and the current of the circuit breaker opening and closing coils. In [18,19], vibration signals are evaluated using SVM and ANN techniques. In addition to the AI and ML techniques mentioned above, there are other signal processing methods, such as the use of the Fourier transform and Wavelet, that also help in predicting and diagnosing circuit breaker failures, like in [20]. In [21], the behavior of the circuit breaker coil current signals during switching is analyzed. In [2,20], several signals from circuit breakers are analyzed using signal processing techniques.

The studies presented generally use computer simulations to determine pre-insertion and main contact points and, consequently, to evaluate the synchronization of the closing phase. However, when data are obtained in real environments, they carry a large amount of noise and interference, making the determination of points difficult. This work proposes the use of artificial intelligence to mitigate this problem so that the solution can be used in any real environment where the circuit breaker is installed. To mitigate this type of problem, this work presents an approach that combines modeling using signal processing and artificial intelligence to automatically find the pre-insertion and main contact points using real current and voltage signals from circuit breakers in an electrical substation, considering all noise and interferences generated in a significant substation environment.

As a contribution of this work, we can highlight (i) the creation and availability of a dataset containing real information for identifying synchronization patterns and other data contained in the current and voltage signals of the high-voltage circuit breakers of a real substation; (ii) the application of machine learning techniques in the context of artificial intelligence for detecting main contact times in current and voltage signals subject to different noise and interferences occurring in a production substation environment; and (iii) statistical analysis providing an overview of synchronization times of the high-voltage circuit breakers of the capacitor banks in the substation.

This article is organized as follows: Section 2 presents the materials and methods, where the steps for implementing the proposed methodology are individually described. In Section 3, the main results demonstrate the evaluations of the artificial intelligence models and/or the outcomes of using the solution on real data from an SF6 circuit breaker bank. Finally, Section 4 presents the conclusions and provides insights for future work.

2. Materials and Methods

The controlled switching of circuit breakers is usually checked during the asset maintenance period in power companies in Brazil, which usually occurs every 6 years, or during corrective maintenance. In the interval between one check and another, due to different factors, variations in the circuit breaker's operating time may occur. It may not close at the optimal timing, which can lead to accelerated wear on the asset and reduce its lifespan. Identifying the contact insertion moments is currently performed visually by a controlled switching specialist. This task becomes complex when considering a real system operating in the substation and subject to various interferences and noises, such as the high transients

generated, as well as the disturbances generated by the back-to-back effect of the controlled switching in the capacitor bank.

In a common signal like Figure 1a, without noise and interference, it is easy to visually identify the pre-insertion, red circle (1), and main contact points, blue circle (2). However, several signals contain noise or interference, which can be caused by defective readings, interference from other closed circuit breaker banks, or even from other phases of the same bank. When the back-to-back effect occurs, it causes high transients. Some examples can be seen on the right side of Figure 1. As can be observed, the main contact identification poses challenges in its location. Even without noise or interference, the point may not be very clear and objective, so any minor incident in the signal greatly hinders its location. Figure 1 shows the issues found in the obtained data, such as high transients in the signal and interference from other closed phases. Using filters to smooth and remove noise has shown some effectiveness, as in each case of noise or interference, one signal filter performs better than another. Thus, using more advanced resources for point identification is necessary.
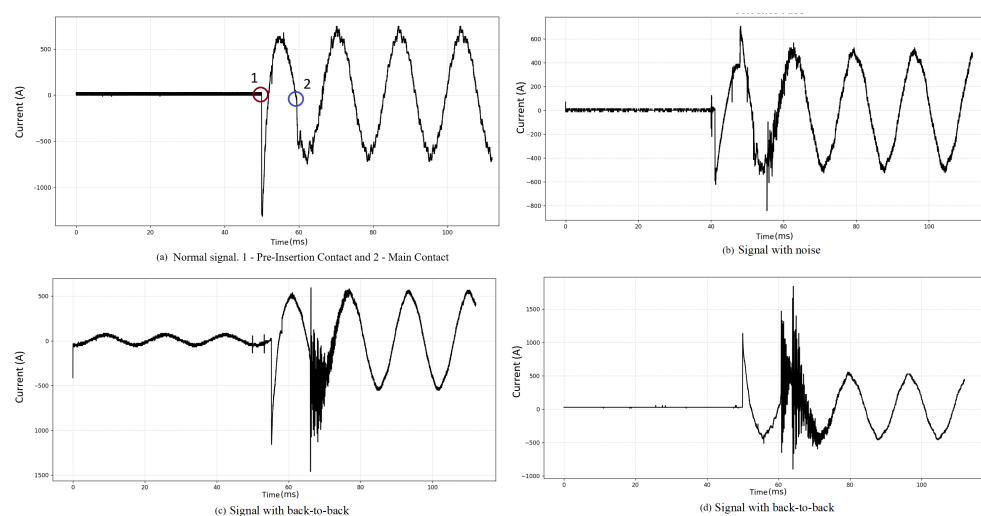
Figure 1. Examples of current signals.

The flowchart in Figure 2 presents the methodology proposed for the development of this work. The development was divided into four modules, characterized by data loading and pre-insertion point detection, dataset generation, model training and testing, and analysis of the circuit breakers operating with a capacitor bank. The first one is responsible for reading the file where the raw current and voltage signals from circuit breakers were saved, applying pre-filtering to detect the pre-insertion point. The second one was structured to transform a processing signal challenge into a classification problem, constructing a dataset by using different filters aimed at feature extraction under noise and several interferences present to detect the point of main contact. The third module was developed to construct two classical classifiers present in the literature to perform the identification of the main contact. After defining the efficient model, the last module is responsible for extracting the times and other information of the circuit breakers to verify synchronism and other information like inrush current, etc. The following subsections will explain in detail what was developed in each module.
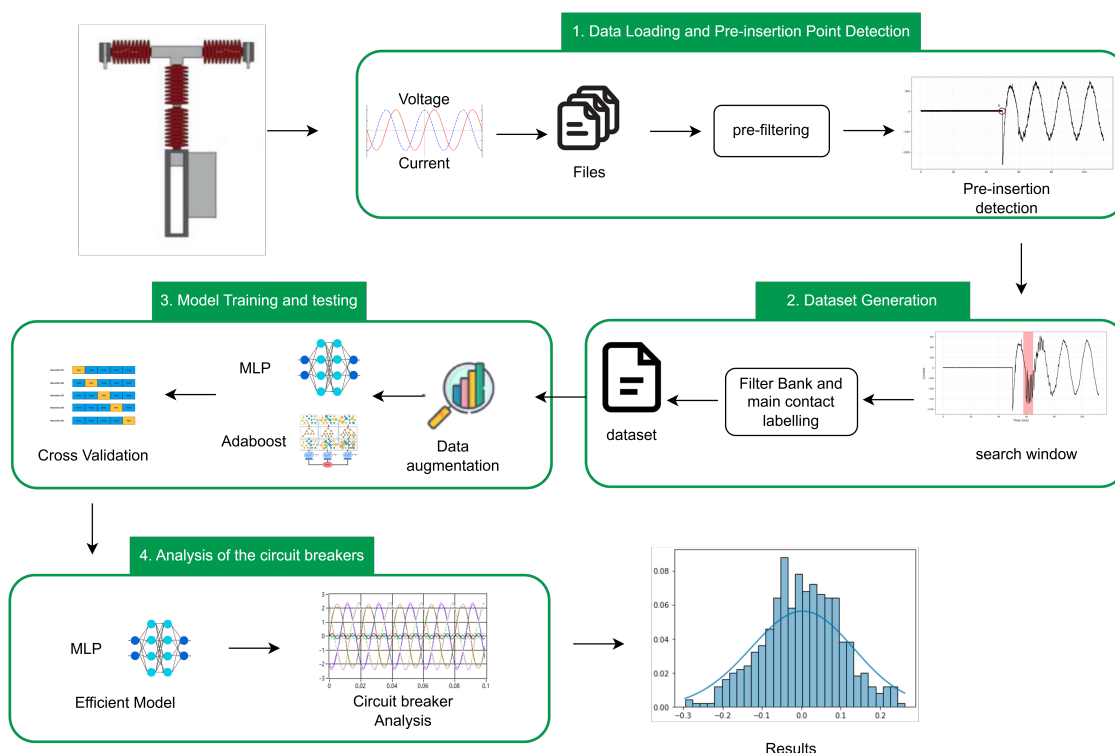
Figure 2. Methodology proposed for the development of this work.

2.1. Data Loading and Pre-Insertion Point Detection

The current and voltage signals were measured directly from the CT and PT secondaries, respectively. These signals were then interfaced with the Advantech PCI-1713U universal PCI board using a Telemulti signal conditioner. The PCI-1713U board, which has 32 isolated analog input channels, was used for data acquisition. With a sampling rate of up to 100 kS/s and a resolution of 12 bits, this board ensures accurate and reliable signal capture. Data capture from capacitor banks occurs each time a bank is operated. Each circuit breaker has three phases that are operated synchronously. The generated file contains the current of all banks and all phases and finally includes the line voltage from phase A to C. Each file contains in its name the date and time the operation took place and the name of the bank that was operated. Therefore, it is at least possible to determine when the operation occurred and which bank was operated. These files have two main issues:

- Corrupted files that cannot be read.
- Files with incorrect bank names: When analyzing the current of the bank named in the file, it is clear that this was not the operated bank, requiring each bank to be checked for identification. For this work, files with this issue were discarded.

The pre-insertion contact can be found, in most cases, by calculating the derivative of the signal. For example, Figure 3a,c presents the raw current signal and its output of the derivative filter. It is possible to see that the first variation is precisely the pre-insertion contact. However, in some cases, only the derivative fails due to noise and interference occurring moments before the pre-insertion point, as in the noise signal example shown in Figure 3b. Thus, its derivative has large prior variations before the pre-insertion contact, requiring a pre-filtering for that. Therefore, a moving average filter represented by Equation (1) was used. $M_i(k)$ represents the smoothed value of the series at point i, calculated using a moving average of order k. k is the number of values used in the moving average calculation; in this case, $k = 10$, meaning the filter considers the last 10 points of the series, and x_{i-j} denotes the value of the series at point $i - j$, where j ranges from 0 to

$k-1$. In other words, these are the most recent values, including the current value (x_i) up to $k-1$ points prior. It smooths the signal, removing previous noise, and proves effective for all test cases.

$$M_i(k) = \frac{1}{k} \sum_{j=0}^{k-1} x_{i-j} \tag{1}$$
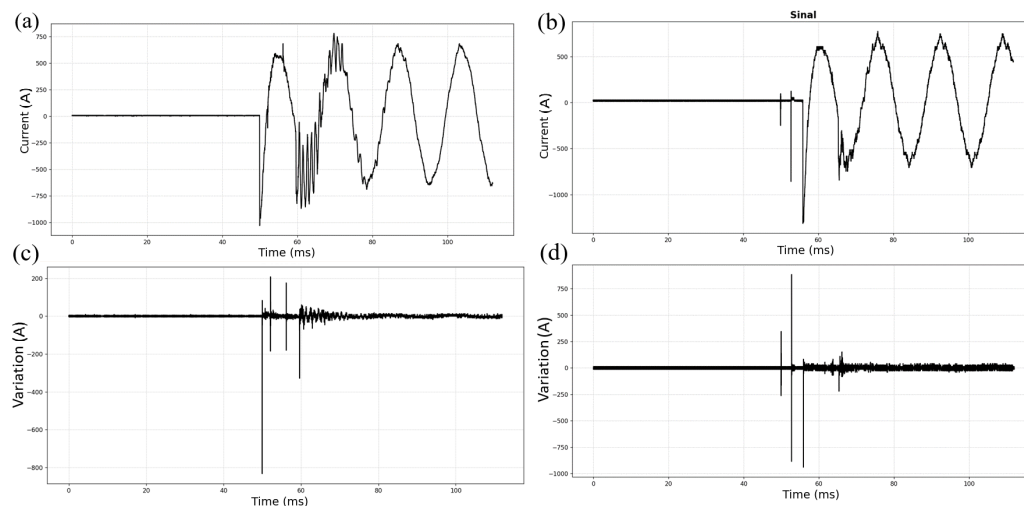
Figure 3. (**a**) Signal without noise. (**b**) Signal with noise. (**c**) Derivative of the signal without noise. (**d**) Derivative of the signal with noise.

2.2. Dataset Generation

The main contact is more challenging to identify in signals with noise and interference. Even with the application of filters to smooth the signal, as in the case of pre-insertion contact, the results obtained are not satisfactory. By processing the signals through a filter bank and organizing each point of the signals sequentially, it becomes possible to construct a training dataset. This approach transforms the challenge into a classification problem, allowing a machine learning model to be trained to identify the main contact with greater accuracy.

To achieve this, the following process was performed. It is known that the circuit breaker manufacturer establishes standard contact time values and allowable variations in well-functioning circuit breakers. The time between pre-insertion and main contact is about 10 ms [10,22]. Thus, using this time as a reference from the pre-insertion contact allows for determining an upward and downward variation, forming a search window in which the main contact may be. This variation was set to 8 ms, a larger variation than considered healthy, which was necessary to include cases where the circuit breaker may be defective. In Figure 4, the window in red on the left provides context for the complete signal, and the right shows the window in detail.

Subsequently, each sample of the signal inside this search window is considered a candidate to be the point of the main contact. In this sense, feature extraction was conducted to characterize the features that can distinguish this main contact under the influence of noise and interferences, as mentioned before. Therefore, several filters with different parameters were applied for that feature extraction process. Table 1 summarizes the filter bank employed and the parameters used for that.
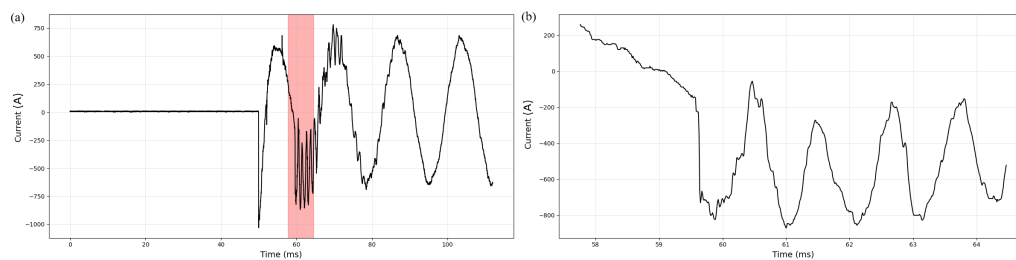
Figure 4. Defining the search window for the main contact. (**a**) The search window was defined from the raw current signal and (**b**) the signal specifically in this window.

Table 1. Table with filters and parameters.

Filter	Parameters
Derivative [23]	Order 1
Integral [23]	Order 1
Moving Average [24]	Convolution with a window size of 10
Median [25]	Using a window size of 10
Savitzky-Golay [26]	With a polynomial of degree 2 and a window size of 10
Fourier Transform [27,28]	Filtering frequencies above 200 Hz
Discrete Cosine Transform [29]	With orthogonal normalization and removing high-frequency components, zeroing the upper half of the coefficients
Hilbert Transform [30]	Calculating the signal envelope and obtaining the signal through the transform's magnitude
Butterworth [31]	With a cutoff frequency of 100 Hz and order 4
Wavelet [32]	Decomposing the signal with different wavelets and keeping only the lowest-level coefficients. Biorthogonal, Coiflet, Discrete Meyer, and Reverse Biorthogonal wavelets were used

In Figure 5, we can observe the original signal and some examples of the applied filters. Note that although each filter smooths the signal, each one exhibits a certain pattern at the moment of contact.
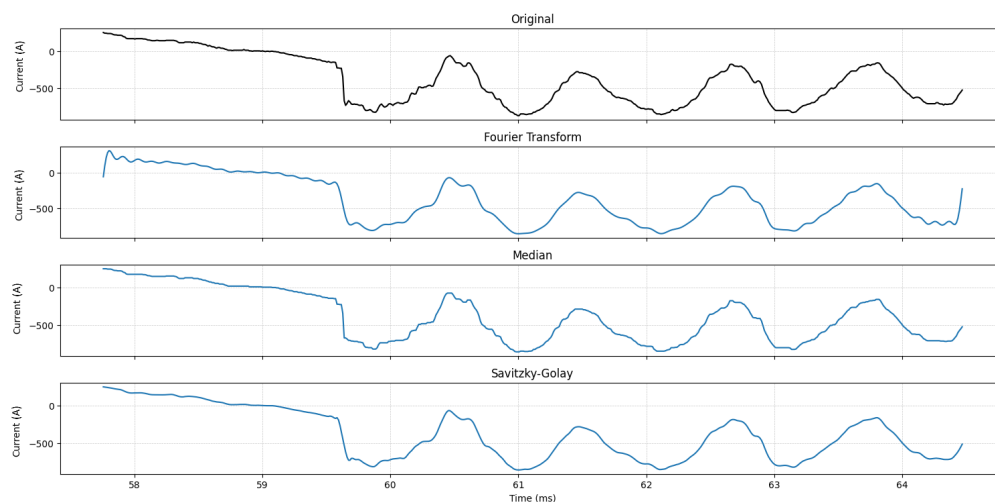
Figure 5. Some responses of the applied filter bank.

Although the voltage signal represents the line-to-line voltage rather than the voltage of each phase individually, it still exhibits identifiable patterns at the pre-insertion and main contact points, as illustrated in Figure 6, where the voltage is represented by the blue line. To leverage this additional information, the voltage signal was included alongside the current signals in the dataset. Both signals are processed using the filter bank developed in this work, resulting in a filtered representation where each filter produces a distinct version of the original signal. Specifically, for each signal type (current and voltage), 41 filters are applied, generating a matrix where each row corresponds to a filtered signal. This matrix is transposed, transforming the columns into the filtered signals, and the resulting feature vector contains 82 columns—41 corresponding to the filtered current signals and 41 to the filtered voltage signals—forming the input for the training dataset. This inclusion aims to enhance the model's ability to identify key events effectively.
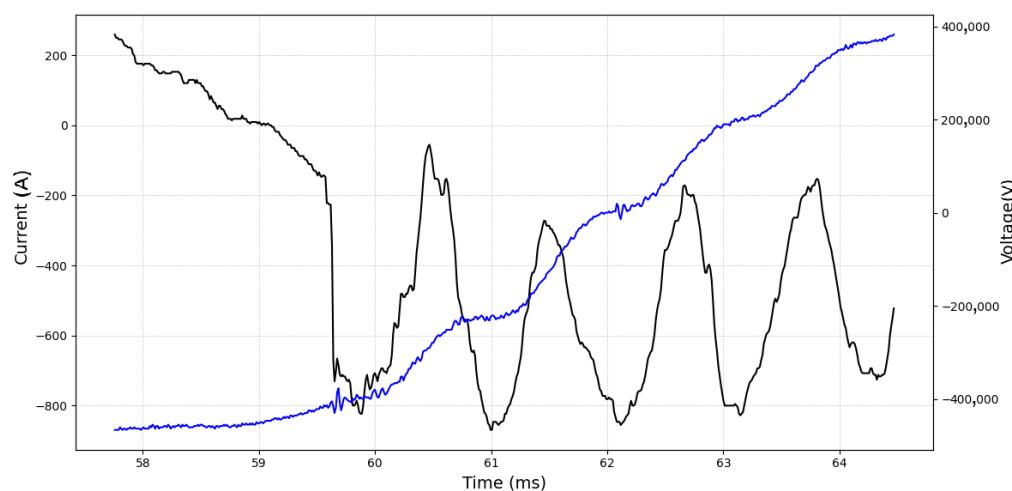
Figure 6. Current and Voltage signals.

The main contact points were manually labeled by visually analyzing each signal in the dataset and precisely marking the point corresponding to the main contact. This approach ensured accurate annotation for the training data (Dataset available at: https://doi.org/10.5281/zenodo.14617420 accessed on 8 January 2025) contains a total of 1,042,199 data points, of which 1737 were labeled as main contact points (value 1) and the remaining as not corresponding to the main contact (value −1). These points come from 1737 signals, distributed by year as shown in the Table 2:

Table 2. Signal distribution in the dataset by year.

Year	Number of Signals
2010	394
2011	584
2019	675
2020	84

2.3. Model Training and Testing

This section provides an overview of the methods employed for training and testing the models. It begins with data augmentation and normalization, covering data balancing techniques and the normalization applied. Following this, the architectures of the multilayer perceptron (MLP) and adaptive boosting (AdaBoost) models are detailed, including training

parameters and the use of k-fold cross-validation. Model performance metrics, such as precision, recall, and F1-score, are presented, along with statistical validation through the Wilcoxon test. Lastly, an analysis of circuit breaker behaviors is conducted, detailing calculations for pre-insertion and main contact timing, maximum inrush current, and phase synchronization, supported by equations and figures.

2.3.1. Data Augmentation and Normalization

The data were prepared through balancing and normalization techniques to ensure data quality during model training. For data balancing, a combination of undersampling and SMOTE (synthetic minority over-sampling technique) [33] was applied. Initially, undersampling was used to reduce the number of incorrect samples. Then, SMOTE was applied to increase the number of correct samples to match the number of incorrect points, resulting in a final dataset of 5000 points that characterize the main contact and the same number of those that don't.

For data normalization, the standardization method was applied using the Standard Scaler technique [34], which transforms each variable X so that its mean is zero and its standard deviation is one, according to Equation (2):

$$X_{\text{normalized}} = \frac{X - \mu}{\sigma} \tag{2}$$

where μ represents the mean of the X values and σ the standard deviation. This step ensures that all variables are on the same scale, improving the effectiveness of the machine learning model.

2.3.2. Multilayer Perceptron—MLP

The MLP is a feedforward neural network composed of an input layer, one or more hidden layers, and an output layer. The network developed in this work has an input layer with 82 neurons, one hidden layer with 100 neurons, and an output layer with 2 neurons, as illustrated in Figure 7. The number of neurons in the input and output layers is determined by the dataset characteristics. The hidden layer, containing 100 neurons, follows the default configuration of the MLPClassifier provided by the Scikit-learn Python library, which is informed by studies that established effective initialization and optimization strategies for neural networks [35–37]. This simple yet effective architecture, coupled with a non-linear activation function such as ReLU, enables the MLP to capture complex relationships within the data. Training is performed using the backpropagation algorithm, which adjusts the weights based on the error at each iteration [38,39].

2.3.3. Adaptive Boosting—AdaBoost

AdaBoost is an ensemble model that combines multiple weak decision trees to form a robust classifier. It utilizes a set of weak classifiers, depth-1 decision trees called stumps, and iterates over them to reduce errors by increasing the weight of misclassified data in each iteration. In this work, the developed model uses 500 estimators, meaning it generates 500 weak classifiers, as illustrated in Figure 8, combining them in a sequence. The parameters follows the default configuration of the AdaBoostClassifier provided by the Scikit-learn library, which is based on prior studies establishing effective strategies for boosting algorithms [40]. Each new classifier attempts to correct the errors of the previous set, adjusting iteratively [41–43].
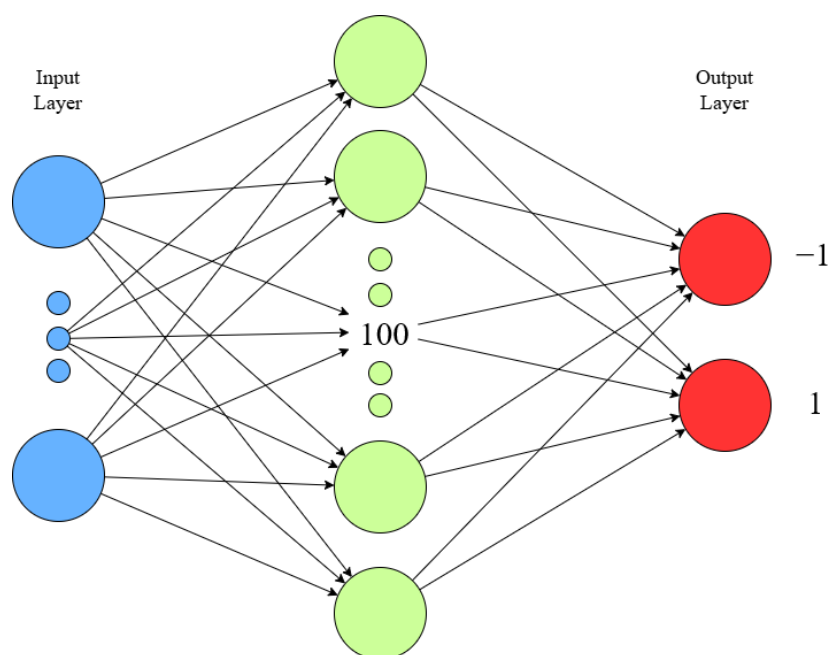
Figure 7. MLP architecture was developed for this work. It has X input neurons, 100 neurons in the hidden layer, and 2 in its output layer.
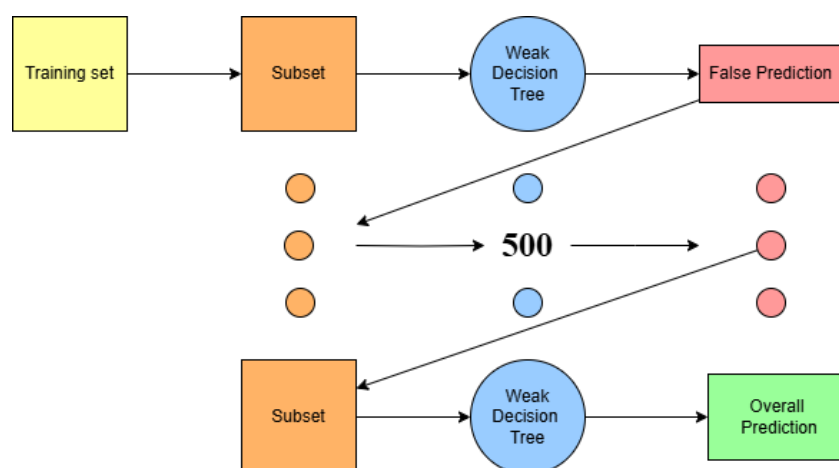

Figure 8. AdaBoost with 500 weak classifiers.

2.4. Cross Validation

To obtain a robust evaluation of model performance, the cross-validation technique was used. This method allows the model to be tested on different subsets of the data, reducing the risk of overfitting or underfitting and ensuring that the observed performance is not specific to a single train-test split. In this work, K-fold cross-validation was employed, where each subset serves as the test set once, while the remaining K-1 subsets form the training set. This process is repeated K times, ensuring that each data instance is used for both training and testing. The parameters used for K-fold cross-validation for both models are presented in Table 3.

Table 3. Parameters Used in K-Fold Cross-Validation.

Parameter	Value
Number of K-Fold splits	10
Seed for reproducibility	42

Model Performance Indicators

The confusion matrix is a table that summarizes the prediction results of a classification model by comparing the model's predictions with the actual values. It consists of four main elements:

- True Positives (TP): Cases where the model correctly predicted the positive class.
- True Negatives (TN): Cases where the model correctly predicted the negative class.
- False Positives (FP): Cases where the model incorrectly predicted the positive class when the actual class was negative (Type I error).
- False Negatives (FN): Cases where the model incorrectly predicted the negative class when the actual class was positive (Type II error).

Based on the confusion matrix, several evaluation metrics can be derived to assess the model's performance in detail [44].

- Accuracy: Accuracy measures the proportion of correct predictions relative to the total predictions made. It is a useful metric when classes are balanced, vide Equation (3).

$$\text{Accuracy} = \frac{TP + TN}{TP + TN + FP + FN} \tag{3}$$

However, in imbalanced datasets, accuracy can be misleading, as a model that always predicts the majority class may have high accuracy but poor performance in capturing the minority class [45].

- Precision: Precision, also known as positive predictive value, measures the proportion of correctly classified positive examples among all examples classified as positive by the model, vide Equation (4).

$$\text{Precision} = \frac{TP}{TP + FP} \tag{4}$$

Precision is especially important in scenarios where false positives should be minimized, such as in medical diagnostics [45,46].

- Recall: Recall, or sensitivity, measures the model's ability to correctly identify all positive examples. It is the proportion of true positives relative to the total examples that actually belong to the positive class, vide Equation (5).

$$\text{Recall} = \frac{TP}{TP + FN} \tag{5}$$

Recall is essential in cases where false negatives should be minimized, such as in detecting severe diseases, where capturing all positive cases is crucial [44,45].

- F1-Score: The F1-score is the harmonic mean of precision and recall, providing a balance between both metrics. It is useful when both precision and recall are important, as shown in Equation (6).

$$F1 = 2 \cdot \frac{\text{Precision} \cdot \text{Recall}}{\text{Precision} + \text{Recall}} \tag{6}$$

The F1-score is more informative than accuracy in imbalanced scenarios, as it balances the importance of true positives and false negatives [44,45].

- Specificity: Measures the proportion of true negatives correctly identified relative to the total examples that actually belong to the negative class, as shown in Equation (7).

$$\text{Specificity} = \frac{TN}{TN + FP} \tag{7}$$

Specificity is relevant in contexts where avoiding false positives is important, such as in screening tests [44].

- Area under the ROC Curve (AUC-ROC): AUC represents the model's ability to distinguish between positive and negative classes. A receiver operating characteristic (ROC) curve is plotted with the x-axis representing the false positive rate and the y-axis representing the true positive rate, as shown in Equation (8).

$$\text{AUC} = \int_0^1 TPR(FPR)\, dFPR \tag{8}$$

A model with an AUC close to 1 is considered excellent, while an AUC of 0.5 indicates no discrimination ability (equivalent to random guessing) [44].

These metrics allow a detailed and rigorous analysis of model performance, ensuring that the results are correctly interpreted in various contexts [47–49].

2.5. Analysis of the Circuit Breakers

In this study, the timing associated with the closing of high-voltage circuit breaker contacts was analyzed to assess the pre-insertion time, main contact, inrush current, and synchronization of the main contact with the current zero-crossing. The method used to extract each of these parameters is detailed below.

To determine the time interval between the pre-insertion contact and the main contact, the pre-insertion contact time ($T_{\text{pre-insertion}}$) was subtracted from the main contact time (T_{main}), as presented in Equation (9):

$$\Delta T_{\text{pre-main}} = T_{\text{main}} - T_{\text{pre-insertion}} \tag{9}$$

where T_{main} represents the moment when the main contact closes, and $T_{\text{pre-insertion}}$ is the time when the pre-insertion contact occurs.

The inrush current value was obtained by finding the peak of the current signal at the moment of the main contact closing. The value of I_{inrush} is described by Equation (10):

$$I_{\text{inrush}} = \max(I(t)) \tag{10}$$

To determine the time interval between the main contact and the current zero-crossing, the current signal was analyzed to identify the zero-crossing points closest to the main contact time, T_{main}. The process involves checking both the preceding and following zero-crossings relative to T_{main}, selecting the closest point. This interval is calculated by the following relation in Equation (11):

$$\Delta T_{\text{zero}} = \min(|T_{\text{main}} - T_{\text{zero,left}}|, |T_{\text{main}} - T_{\text{zero,right}}|) \tag{11}$$

where $T_{\text{zero,left}}$ and $T_{\text{zero,right}}$ represent the times of the nearest zero-crossings before and after T_{main}, respectively.

In three-phase systems, each phase (A, B, and C) must close in sync with a 60-degree (2.78 ms) phase difference, which is crucial to prevent unwanted current transients and maintain system balance. To evaluate the synchronization in the closing of the main contacts between phases A, B, and C, we calculated the time intervals between the main contact closing moments of each phase. The synchronization is defined by the time differences between the main contacts of the adjacent phases, as shown in Equations (12) and (13):

$$\Delta T_{\text{sync,AB}} = T_{\text{principal,B}} - T_{\text{principal,A}} \tag{12}$$

$$\Delta T_{\text{sync,BC}} = T_{\text{principal,C}} - T_{\text{principal,B}} \tag{13}$$

A total of 4795 files were analyzed, each containing the signal from three phases, resulting in 14,385 signals. The pre-insertion contact time, main contact time, difference between them, synchronization time of the main contact with the current zero-crossing, the maximum current value of the signal, and the synchronization between phases were calculated.

3. Results

This section presents and discusses the results obtained from the analysis of circuit breaker current signals, covering both the performance of training and validation models as well as the statistical analysis of circuit breaker operation times. The analysis is divided into two main subsections: the first examines the effectiveness of the models used, including quantitative and qualitative metrics of the detections made, while the second subsection explores temporal and current aspects of the events, such as the time between pre-insertion and main contact, maximum inrush current, and the synchronization of phases A, B, and C. For clarity, tables and figures are presented to illustrate the evaluated variables, providing a comprehensive overview of circuit breaker behavior under different operating conditions.

3.1. Training and Validation Analysis of the Models

The MLP network developed has a single hidden layer with 100 neurons, configured with the ReLU (Rectified Linear Unit) activation function. The initial learning rate was set to 0.001 and remained constant throughout the training process. The optimization algorithm used was Adam, which combines the advantages of stochastic gradient with momentum adaptations. The maximum number of epochs was fixed at 300, and the stopping criterion was based on the minimum variation in loss, with a tolerance of 0.0001. The regularization rate was set to 0.0001, and a momentum value of 0.9 was applied to smooth the weight updates. The model was also configured to allow early stopping if there was no significant improvement in the loss over 10 consecutive iterations.

The AdaBoost model was configured to use the SAMME.R algorithm, which adjusts sample weights based on the accumulated error rate of each weak estimator. The learning rate was set to 1.0, keeping the impact of each estimator uniform throughout the training process. The maximum number of estimators was set to 500, indicating that AdaBoost will add up to 500 weak estimators to improve the final model's performance. The default base estimator used was a decision tree, and the random state parameter was set to 42 to ensure reproducibility of the results.

The models were evaluated based on all parameters mentioned in Section 2.4, and the average values after cross-validation can be seen in Table 4.

Table 4. Model Performance Metrics.

Model	Accuracy	Precision	F1 Score	Recall	Specificity	AUC-ROC
AdaBoost	0.9523	0.9524	0.9523	0.9523	0.9540	0.9857
MLP	0.9468	0.9470	0.9468	0.9468	0.9449	0.9842

The Wilcoxon signed-rank test was conducted to compare the overall performance metrics (Accuracy, Precision, F1 Score, Recall, Specificity, and AUC-ROC) between the AdaBoost and MLP models, shown in Figure 9. The test yielded a test statistic of 0.0 and a p-value of 0.03125, indicating a statistically significant difference between the two models' performance at the 5% significance level. This result suggests that the AdaBoost and MLP models do not perform identically across all evaluated metrics, with AdaBoost demonstrating a slight overall advantage in this analysis.
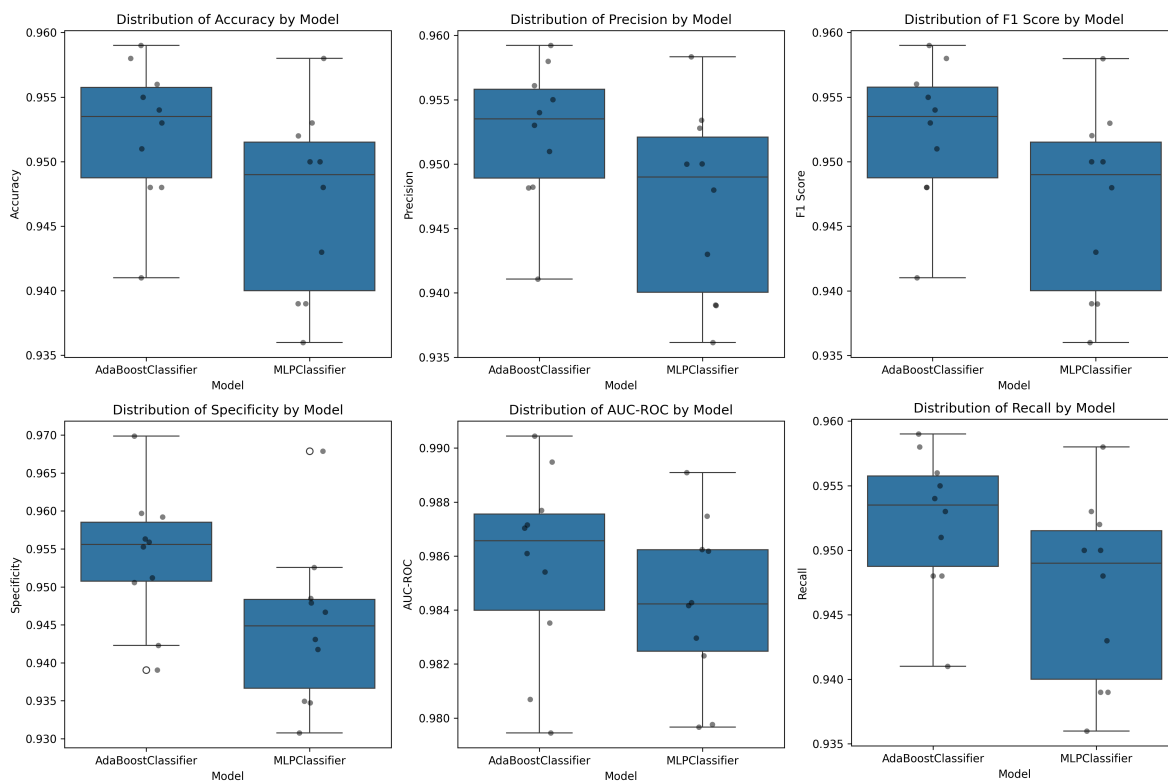
Figure 9. Model Evaluation.

The learning curve of the AdaBoost model, shown in Figure 10, and the curve of MLP, shown in Figure 11, illustrate the model's stability in terms of accuracy. The x-axis in each learning curve represents the training set size, the fraction or number of samples used to train the model at each point. The training line indicates the model's accuracy on the training set for each training size, and the validation line shows the model's accuracy on a separate validation set. When the training and validation lines are close and stable, the model achieves a good balance, effectively capturing patterns without overfitting to the training data.
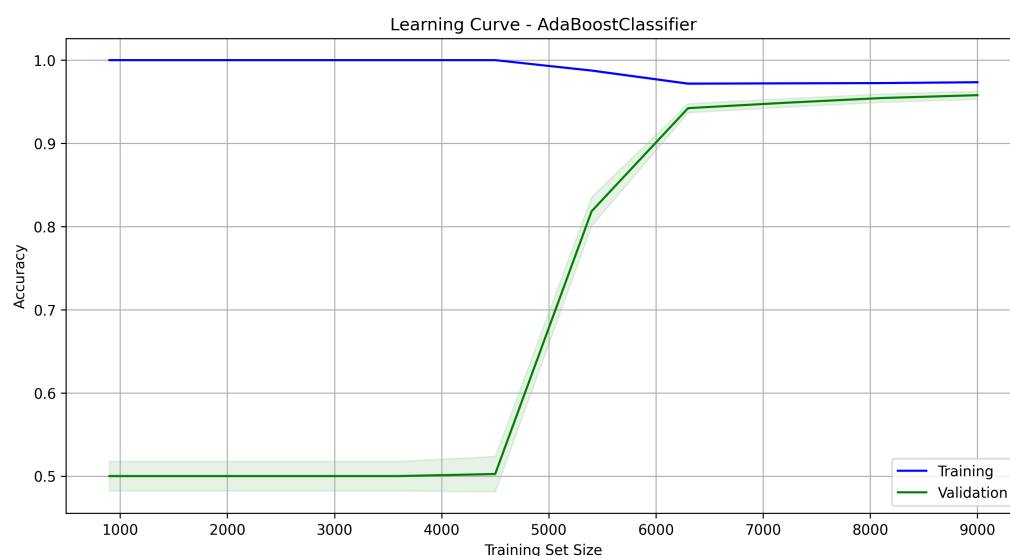
Figure 10. AdaBoost Learning Curve.

Thus, the AdaBoost model was selected for identifying the main contact. Figure 12 shows the results of the automatic identifications, where the black line represents the pre-insertion contact, and red indicates the main contact.
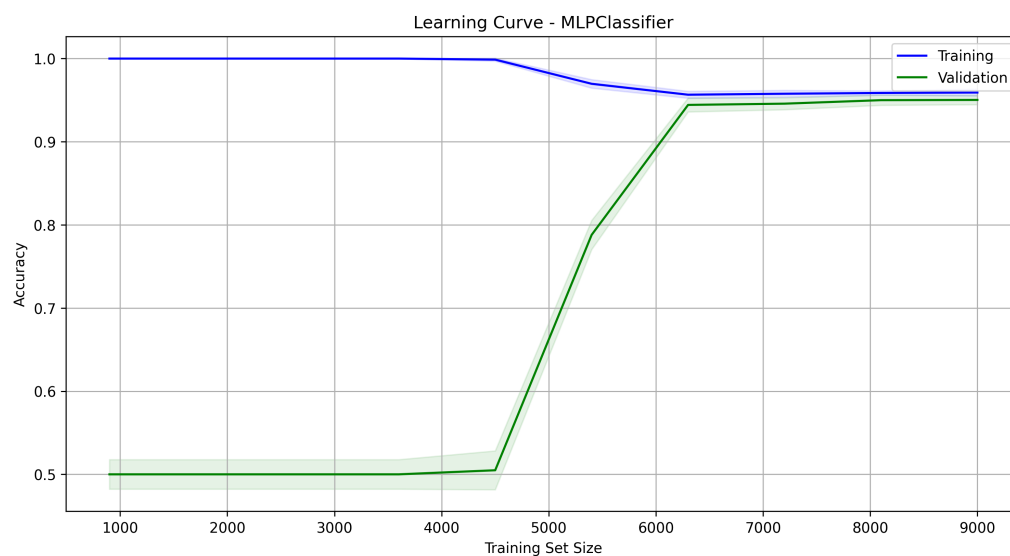
Figure 11. MLP Learning Curve.
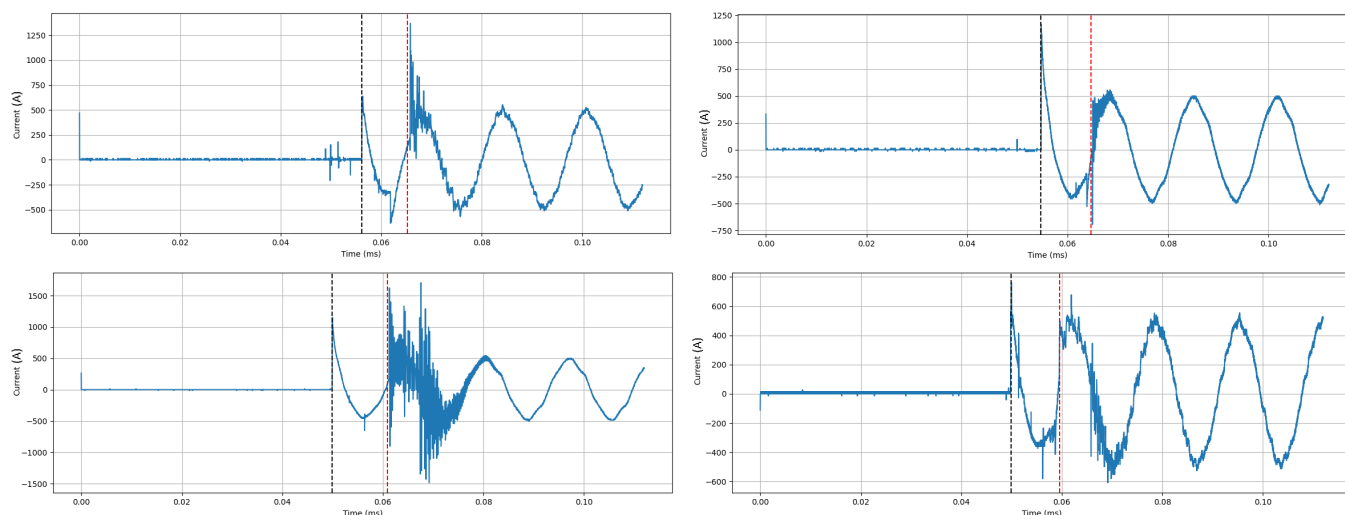
Figure 12. Automatically Marked Signals.

3.2. Statistical Analysis of Circuit Breaker Timing

The interval between contacts, which, according to the manufacturer, should remain around 10 ms, was within the expected range in most cases [10,22]. However, a significant number of cases showed this value between 9 ms and 10 ms. These values can be seen in Figure 13.

When analyzing the inrush current, it can be seen in Figure 14 that, recently, in 2020, this maximum was significantly reduced, possibly indicating some type of improvement in the equipment or control mechanism to prevent peak currents in the circuit breakers.

Another point to highlight is the inrush current in relation to phases, shown in Figure 15, where the first phase has higher values than the other phases, and the last phase has lower values.
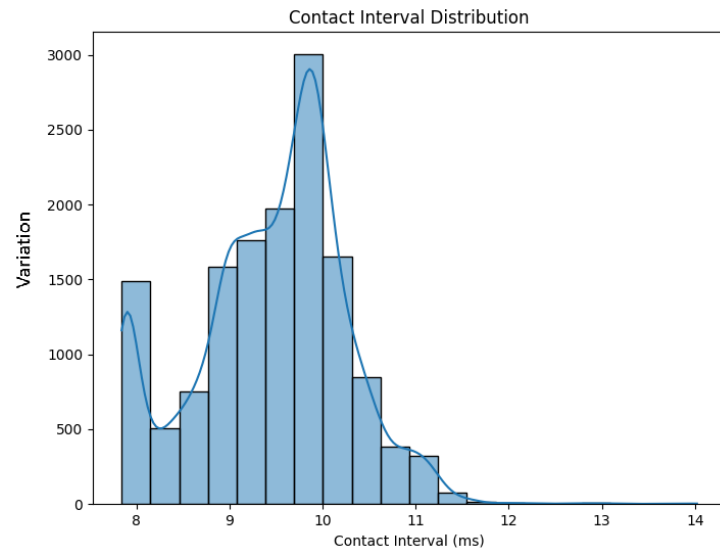
Figure 13. Contact Interval Distribution.
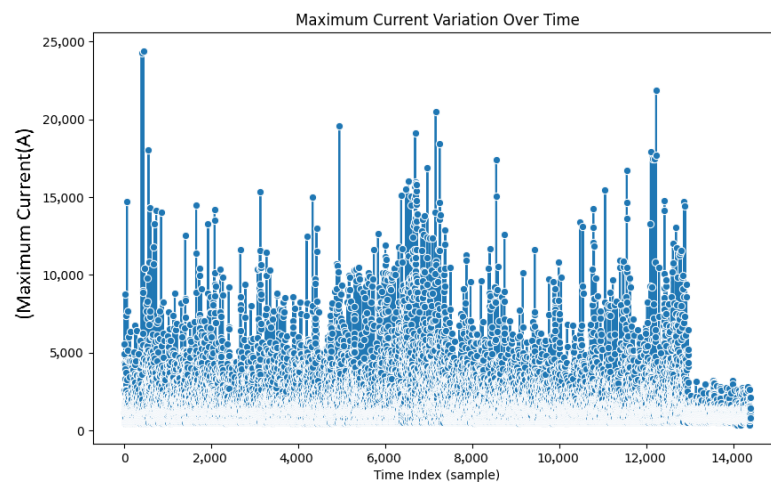
Figure 14. Inrush over years.
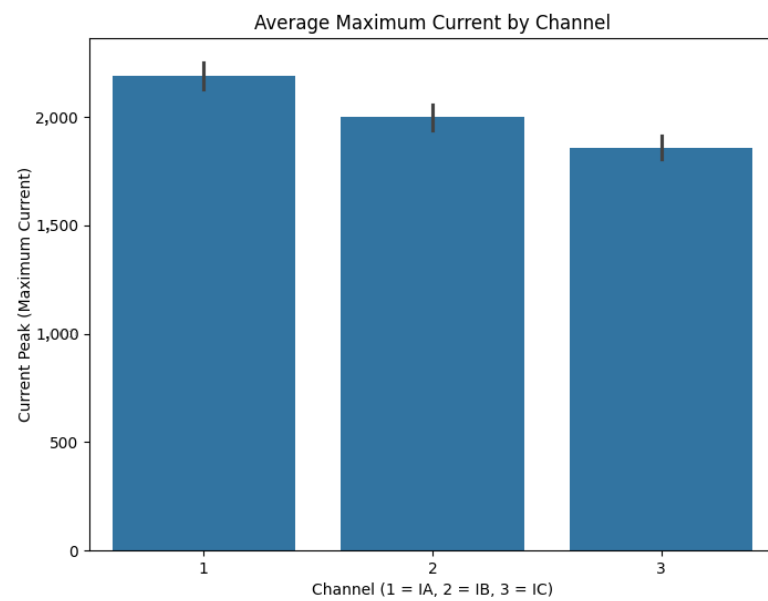
Figure 15. Inrush and Phases.

When analyzing the interval between the main contact and the current zero-crossing, it can be observed in Figure 16 that the synchronization is correct in most data, with outliers being a point of attention.
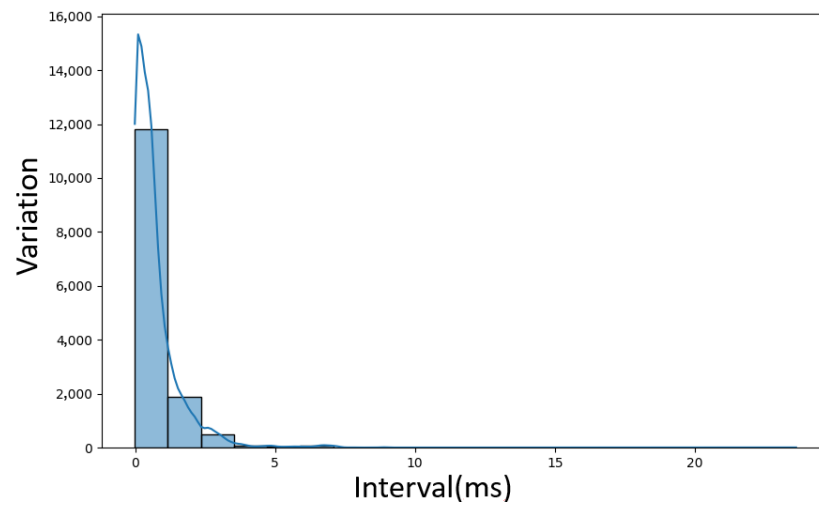

Figure 16. Interval between main contact and current zero-crossing.

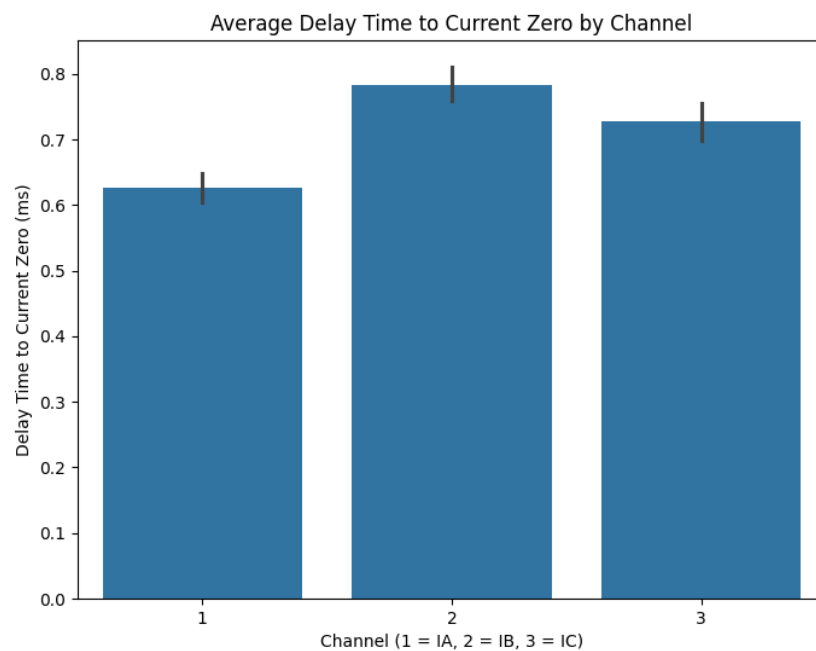Grouping by channel shows that phase B is more out of sync than the other phases, as evidenced in Figure 17.

Figure 17. Phases interval between main contact and current zero-crossing.

The synchronization among phases is illustrated in Figure 18, where an evident average value can be observed, indicating that synchronization is generally within healthy levels. The outliers highlight a point of attention that may indicate potential issues.
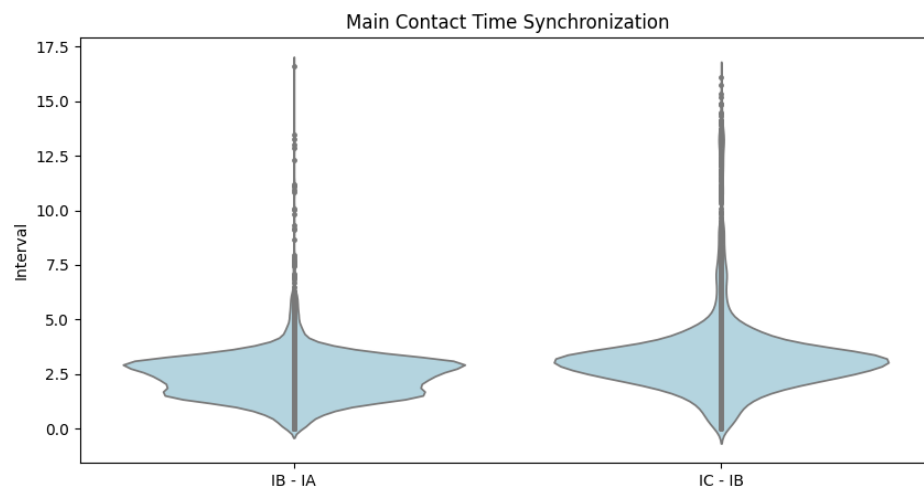
Figure 18. Phases Synchronization.

4. Conclusions

This work addressed a significant challenge in the field of high-voltage circuit breakers: the precise identification of pre-insertion and main contact points during closing operations. The complexity of this problem lies in the need to handle noisy signals and operating environments that can compromise the accuracy of conventional analyses. Current and voltage data collected from real environments subject to significant noise and interference were processed, and the results showed that the proposed method achieved an accuracy above 90% in identifying the main contact points, proving its effectiveness even in scenarios with high levels of noise. The main contribution of this work is the demonstration that the integration of signal processing methods and machine learning can be successfully applied to enhance the identification of features in current and voltage signals in high-voltage circuit breakers. This methodology can also be extended and adapted to different types of signals extracted from circuit breakers, such as vibration. For future work, it is proposed to explore the use of more complex neural network architectures, such as convolutional neural networks, to further improve the accuracy and generalization capacity of the models. Additionally, incorporating the solution into real-time monitoring systems may represent a promising expansion, allowing immediate responses to critical variations and early detection of potential failures, as well as the instant adjustment of Switching controllers.

Author Contributions: Conceptualization; Methodology; Software; Validation; Formal Analysis; Investigation: P.A.V.D.L. and G.B.V.; Writing, Review and Editing: P.A.V.D.L., G.B.V., R.T.L., A.L.M.C. and E.P.S.; Resources; Visualization; Supervision; Project Administration and Funding Acquisition: G.B.V. All authors have read and agreed to the published version of the manuscript.

Data Availability Statement: The link to access the data is contained in the article.

Conflicts of Interest: Ricardo T. Lima employed by Centrais Elétricas Brasileiras S/A —ELETRO-BRÁS. The remaining authors declare that the research was conducted in the absence of any commercial or financial relationships that could be construed as a potential conflict of interest.

Abbreviations

The following abbreviations are used in this manuscript:

AI	Artificial Intelligence
PIR	Pre-insertion Resistor

DCT	Discrete Cosine Transform
AUC-ROC	Area Under the Receiver Operating Characteristic Curve
MLP	Multi-Layer Perceptron
ReLU	Rectified Linear Unit
AdaBoost	Adaptive Boosting
TP	True Positives
TN	True Negatives
FP	False Positives
FN	False Negatives

References

1. Gao, W.; Qiao, S.P.; Wai, R.J.; Guo, M.F. A Newly Designed Diagnostic Method for Mechanical Faults of High-Voltage Circuit Breakers via SSAE and IELM. *IEEE Trans. Instrum. Meas.* **2021**, *70*, 3500613. [CrossRef]
2. Razi-Kazemi, A.A.; Niayesh, K. Condition Monitoring of High Voltage Circuit Breakers: Past to Future. *IEEE Trans. Power Deliv.* **2021**, *36*, 740–750. [CrossRef]
3. Bao, M.; Li, Y.; Zhao, Y.; Peng, H.; Li, J.; Chen, Z.; Liu, G. Research on High Frequency Induced Current Based High Voltage Circuit Breaker Opening and Closing Time Testing Method. In Proceedings of the Conference: 2024 7th Asia Conference on Energy and Electrical Engineering (ACEEE), Chengdu, China, 20–22 July 2024; pp. 52–56. [CrossRef]
4. Panda, S.; Bahirat, H.; Stanek, M. Controlled switching of power circuit breakers. In Proceedings of the 2016 IEEE International Conference on Power System Technology (POWERCON), Wollongong, NSW, Australia, 28 September–1 October 2016; pp. 1–6. [CrossRef]
5. Eng, M.; Gutierrez Eng, A. Controlled switching and circuit breaker monitoring. In Proceedings of the 2017 IEEE 37th Central America and Panama Convention (CONCAPAN XXXVII), Managua, Nicaragua, 15–17 November 2017; pp. 1–5. [CrossRef]
6. CIGRE. *Guidelines and Best Practices for the Commissioning and Operation of Controlled Switching Projects*; Technical Report 757, CIGRE Technical Brochure; CIGRE: Paris, France, 2019.
7. IEEE. *Guide for the Application of Shunt Power Capacitors*; IEEE: Piscataway, NJ, USA, 2021. [CrossRef]
8. IEEE. *Guide for the Application of Capacitive Current Switching for AC High-Voltage Circuit Breakers Above 1000 V*; IEEE: Piscataway, NJ, USA, 2023. [CrossRef]
9. IEEE. *Draft Standard Test Procedures for AC High-Voltage Circuit Breakers with Rated Maximum Voltage Above 1000 V Amendment 1: Modifications to Test Procedures*; IEEE: Piscataway, NJ, USA, 2024. [CrossRef]
10. Zondi, S.; Bokoro, P.; Paul, B. EMTP-based analysis of pre-insertion resistor and point on wave switching methodology. In Proceedings of the AFRICON 2015, Addis Ababa, Ethiopia, 14–17 September 2015; IEEE: Piscataway, NJ, USA, 2015; pp. 1–5.
11. Luz, G.S.; Arentz, D.S.; Junior, A.R.; Piantino, E.A.; Dias, J.B.; Braz, V.W.; Junior, A.D.P. Adjustment of Synchronizers in the Closing Maneuver of the Capacitor Banks of the Tijuco Preto Substation. In Proceedings of the XIII 401 Eriac-Ibero-American Regional Meeting of CIGRÉ, Puerto Iguazú, Argentina, 24–28 May 2009.
12. Goldsworthy, D.; Roseburg, T.; Tziouvaras, D.; Pope, J. Controlled Switching of HVAC Circuit Breakers: Application Examples and Benefits. In Proceedings of the 2008 61st Annual Conference for Protective Relay Engineers, College Station, TX, USA, 1–3 April 2008; pp. 520–535. [CrossRef]
13. Sun, R.; McVey, M.; Yang, D.; Stage, J.R. A Study of Synchronous Breaker Switching With Preinsertion Resistor for Capacitors Banks. *IEEE Trans. Power Deliv.* **2018**, *33*, 821–829. [CrossRef]
14. Liu, A.; Wu, Z.; Wang, Y.; Ma, S. A Novel Control Strategy of Phase-Controlled Switching Technology for Vacuum Circuit Breaker. *IEEE Access* **2022**, *10*, 43571–43582. [CrossRef]
15. Silva, M. Monitoring System and Methodology to Estimation of Circuit Breaker Operation Times. Ph.D. Thesis, Polytechnic School of the University of São Paulo, São Paulo, Brazil, 2005.
16. Razi-Kazemi, A.A.; Vakilian, M.; Niayesh, K.; Lehtonen, M. Circuit-Breaker Automated Failure Tracking Based on Coil Current Signature. *IEEE Trans. Power Deliv.* **2014**, *29*, 283–290. [CrossRef]
17. Razi-Kazemi, A. Applicability of auxiliary contacts in circuit breaker online condition assessment. *Electr. Power Syst. Res.* **2015**, *128*, 53–59. [CrossRef]
18. Gao, W.; Wai, R.J.; Qiao, S.P.; Guo, M.F. Mechanical Faults Diagnosis of High-Voltage Circuit Breaker via Hybrid Features and Integrated Extreme Learning Machine. *IEEE Access* **2019**, *7*, 60091–60103. [CrossRef]
19. Zhou, Y.; Xue, Y.; Zhou, K. Failure analysis of arc ablated tungsten-copper electrical contacts. *Vacuum* **2019**, *164*, 390–395. [CrossRef]
20. Ji, T.; Yi, L.; Tang, W.; Shi, M.; Wu, Q.H. Multi-mapping fault diagnosis of high voltage circuit breaker based on mathematical morphology and wavelet entropy. *CSEE J. Power Energy Syst.* **2019**, *5*, 130–138. [CrossRef]

21. Hosseini, M.; Stephen, B.; McArthur, S.D.; Helm, J. Current-Based Trip Coil Analysis of Circuit Breakers for Fault Diagnosis. In Proceedings of the 2018 IEEE PES Innovative Smart Grid Technologies Conference Europe (ISGT-Europe), Sarajevo, Bosnia and Herzegovina, 21–25 October 2018; pp. 1–6. [CrossRef]

22. Fantozzi, G.V. Selecting a capacitor-switching overvoltage control method effective in preventing nuisance tripping of adjustable-speed drives. In Proceedings of the EEI ES&E Committee Meeting, Clearwater Beach, FL, USA, 4 April 1995.

23. Salinas, M.; Salas, R.; Mellado, D.; Glaría, A.; Saavedra, C. A Computational Fractional Signal Derivative Method. *Model. Simul. Eng.* **2018**, *2018*, 7280306. [CrossRef]

24. Shan, Z.; Yang, J.; Sanjuán, M.A.F.; Wu, C.; Liu, H. A Novel Adaptive Moving Average Method for Signal Denoising in Strong Noise Background. *Eur. Phys. J. Plus* **2022**, *137*, 50. [CrossRef]

25. George, G.; Oommen, R.M.; Shelly, S.; Philipose, S.S.; Varghese, A.M. A Survey on Various Median Filtering Techniques For Removal of Impulse Noise From Digital Image. In Proceedings of the 2018 Conference on Emerging Devices and Smart Systems (ICEDSS), Tiruchengode, India, 2–3 March 2018; pp. 235–238. [CrossRef]

26. Savitzky, A.; Golay, M.J.E. Smoothing and Differentiation of Data by Simplified Least Squares Procedures. *Anal. Chem.* **1964**, *36*, 1627–1639. [CrossRef]

27. Fourier, J. *La Théorie Analytique de la Chaleur*; Chez Firmin Didot, Père et Fils: Paris, France, 1822.

28. Gonzalez, R.C.; Woods, R.E. *Digital Image Processing*, 4th ed.; Pearson Education Limited: Essex, UK, 2018.

29. Zhou, J.; Chen, P. Generalized Discrete Cosine Transform. In Proceedings of the 2009 Pacific-Asia Conference on Circuits, Communications and Systems, Chengdu, China, 16–17 May 2009; pp. 449–452. [CrossRef]

30. Feldman, M. Hilbert transform in vibration analysis. *Mech. Syst. Signal Process.* **2011**, *25*, 735–802. [CrossRef]

31. Shouran, M.; Elgamli, E. Design and Implementation of Butterworth Filter. *Int. J. Innov. Res. Sci. Eng. Technol.* **2020**, *9*, 7975.

32. Caumo, L. Application and Calculation of the Derivative of Industrial Process Signals. Master's Dissertation, Federal University of Rio Grande do Sul, Porto Alegre, Brasil, 2006.

33. Fernández, A.; Garcia, S.; Herrera, F.; Chawla, N.V. SMOTE for learning from imbalanced data: Progress and challenges, marking the 15-year anniversary. *J. Artif. Intell. Res.* **2018**, *61*, 863–905. [CrossRef]

34. Raju, V.G.; Lakshmi, K.P.; Jain, V.M.; Kalidindi, A.; Padma, V. Study the influence of normalization/transformation process on the accuracy of supervised classification. In Proceedings of the 2020 Third International Conference on Smart Systems and Inventive Technology (ICSSIT), Tirunelveli, India, 20–22 August 2020; IEEE: Piscataway, NJ, USA, 2020; pp. 729–735.

35. He, K.; Zhang, X.; Ren, S.; Sun, J. Delving Deep into Rectifiers: Surpassing Human-Level Performance on ImageNet Classification. In Proceedings of the 2015 IEEE International Conference on Computer Vision (ICCV), Santiago, Chile, 7–13 December 2015; pp. 1026–1034. [CrossRef]

36. Kingma, D.; Ba, J. Adam: A Method for Stochastic Optimization. In Proceedings of the International Conference on Learning Representations, Banff, AB, Canada, 14–16 April 2014.

37. Glorot, X.; Bengio, Y. Understanding the difficulty of training deep feedforward neural networks. In Proceedings of the Thirteenth International Conference on Artificial Intelligence and Statistics, Chia Laguna Resort, Sardinia, Italy, 13–15 May 2010; Teh, Y.W., Titterington, M., Eds.; Proceedings of Machine Learning Research: Cambridge, MA, USA, 2010; Volume 9, pp. 249–256.

38. Delashmit, W.H.; Manry, M.T. Recent developments in multilayer perceptron neural networks. In Proceedings of the Seventh Annual Memphis Area Engineering and Science Conference, MAESC, Memphis, TN, USA, 11–13 May 2005; Volume 7, p. 33.

39. Popescu, M.C.; Balas, V.E.; Perescu-Popescu, L.; Mastorakis, N. Multilayer perceptron and neural networks. *WSEAS Trans. Circuits Syst.* **2009**, *8*, 579–588.

40. Rosset, S.; Zou, H.; Hastie, T. Multi-class AdaBoost. *Stat. Its Interface* **2006**, *2*, 349–360. [CrossRef]

41. Schapire, R.E. Explaining AdaBoost. In *Empirical Inference: Festschrift in Honor of Vladimir N. Vapnik*; Schölkopf, B., Luo, Z., Vovk, V., Eds.; Springer: Berlin/Heidelberg, Germany, 2013; pp. 37–52. [CrossRef]

42. Wyner, A.J.; Olson, M.; Bleich, J.; Mease, D. Explaining the success of adaboost and random forests as interpolating classifiers. *J. Mach. Learn. Res.* **2017**, *18*, 1–33.

43. An, T.K.; Kim, M.H. A new diverse AdaBoost classifier. In Proceedings of the 2010 International Conference on Artificial Intelligence and Computational Intelligence, Sanya, China, 23–24 October 2010; IEEE: Piscataway, NJ, USA, 2010, Volume 1, pp. 359–363.

44. Yacouby, R.; Axman, D. Probabilistic Extension of Precision, Recall, and F1 Score for More Thorough Evaluation of Classification Models. In Proceedings of the First Workshop on Evaluation and Comparison of NLP Systems, Online, 12 November 2020; Eger, S., Gao, Y., Peyrard, M., Zhao, W., Hovy, E., Eds.; pp. 79–91. [CrossRef]

45. Flach, P. Performance Evaluation in Machine Learning: The Good, the Bad, the Ugly, and the Way Forward. In Proceedings of the AAAI Conference on Artificial Intelligence 2019, Honolulu, HI, USA, 27 January–1 February 2019; Volume 33, pp. 9808–9814. [CrossRef]

46. Simon, G.J.; Aliferis, C. (Eds.) *Artificial Intelligence and Machine Learning in Health Care and Medical Sciences*, 1st ed.; Health Informatics, Springer: Cham, Switzerland, 2024; Volume XXVI, 810p. [CrossRef]

47.   Ying, X. An Overview of Overfitting and its Solutions. *J. Phys. Conf. Ser.* **2019**, *1168*, 022022. [CrossRef]
48.   Anguita, D.; Ghelardoni, L.; Ghio, A.; Oneto, L.; Ridella, S. The'K'in K-fold Cross Validation. In Proceedings of the ESANN, Bruges, Belgium, 25–27 April 2012; Volume 102, pp. 441–446.
49.   Zhang, X.; Liu, C.A. Model averaging prediction by K-fold cross-validation. *J. Econom.* **2023**, *235*, 280–301. [CrossRef]